Shapeshift 3D Repair™ – A fully Automated and Unsupervised Cloud API for the Reliable Reconstruction of Raw 3D Surface Scans Data

Patrick LAURIN, Daniel BÉLAND, Jonathan BORDUAS*
Technologies ShapeShift 3D Inc., Montréal (QC), Canada

https://doi.org/10.15221/19.015

Abstract

This paper presents a study to quantify the reliability of the automatic reconstruction tool Shapeshift 3D Repair™ to create watertight, genus 0, precise and accurate 3D surface scan of the human body. Our methodology uses a precise baseline 3D scan acquired from a full body 3D scanner as an input of a scanning process simulator that emulates the properties of a common 3D scanner, the Structure™ by Occipital™, and the behavior of a typical untrained handheld 3D scanner operator. The output of the simulator is a raw scan (noisy and incomplete). Afterward, the raw scan is fed to Shapeshift 3D Repair™ which outputs a reconstructed scan. We express the reliability of the process in terms of Standard Error of Measurement (SEM). Using the girth difference between the baseline scan and the reconstructed scan, we express the compatibility in terms of Signed Mean Difference (Bias) and Mean Absolute Error (MAE). We compare our results with common reconstruction methods found in the literature and with other studies about the reliability of 3D Scanning, Plaster Casting and Traditional Anthropometry.

Context: To create custom medical devices and wearables, the patient's 3D geometry can be acquired using a 3D scanner. The raw 3D scans require post-processing as they are often noisy and incomplete. While organizations using 3D scanners put in place training programs, scans are often of poor quality. To this day, this issue is a hindrance to business models centered on 3D scanning such as the novel 3Dscan-to-3Dprint business model; inadequate scans must be manually corrected by the operators, which is a time-consuming offline process. The study is focused on the simulation of the scanning process and the scan reconstruction of the knee.

Results: A fully automated and unsupervised cloud processing service for the reconstruction of the knee has been implemented and is ready to be tested by users and vendors of 3D scanners. Reconstructed scans exhibit leg, knee and max thigh girth error under 0.1 cm, 0.3 cm and 0.4 cm respectively with 95% confidence level while producing properly defined surface that are manifold, genus 0, have good triangle aspect ratio, and have a single surface. With the recent boom of devices featuring an embedded 3D scanner, we believe that in due time, our technology can be accessible to millions of users without the needs of industry-specific hardware or skills.

Keywords: Digital anthropometry, 3D reconstruction, 3D scanning, cloud computing, API, measurements, accuracy, reliability, compatibility, 3D reconstruction, MAD, SEM, Bias, MAE, ICC.

1. Introduction

Commons method for measuring bodies for custom ergonomic products are Traditional Anthropometry (TA), Plaster Casting (PC) and 3D scanning (3DS). The reliability of TA usually relies on the training of the user and systematic biases between trained users has been observed [1]–[4]. PC produce unreliable results [52] as soft tissue tends to distort under pressure and the removing of the cast, which reduces the repeatability and reliability of the process as it creates additional distortion [5]. Contrary to TA and 3DS, PC requires shipping if the custom products are centrally fabricated off-site. The shipping can further distort the shape capture medium and induce delay in the fabrication. Besides PC is significantly more time consuming than 3DS; cost benefit analysis showed that plaster casting takes 11 minutes on average per event, while foot shape capture through 3DS takes 2 minutes on average per event [6].

3DS devices have grown in popularity as they are more practical than TA and more reliable than PC [7], [8]. They allow to capture the actual body shapes, and not just measurements, to create products such as high-performance 3D orthoses and prostheses [9]–[15]. We can group 3D scanning devices into two groups, handheld and full body scanners. Stationary, full body, scanners are reliable and not operator dependent, but they are bulky, impractical to move, expensive and require the often-injured patient to be brought to the scanner, as opposed to handheld ones. As such, their use has been mostly limited to research purposes and high precision capture for the entertainment industry [16].

* jonathan.borduas@shapeshift3D.com; shapeshift3D.com

On the other hand, low-cost handheld 3D scanner use is now common throughout medical applications (such as orthotics and prosthetics O&P), clothing applications and research as they can be used in various settings [17]. The penetration of 3DS into custom orthotics varies from region to region, the amount of podiatrists using 3DS instead of traditional methods to capture the patient's foot shape is estimated to be 41% in Australia and 13% in the UK [18]. Like TA and PC, handheld 3DS also shows a dependency on the skills of the operator while introducing new source of errors linked to the hardware technical specifications such as resolution, 3D accuracy of the scanner and methods of data processing [19]. Raw 3D scans from handheld devices most certainly require post-processing as they are noisy, incomplete and contain unwanted data from the surroundings [20]–[22]. While organizations using 3D scanners put in place training programs, scans regularly exhibits flaws including, but not limited to, voids and missing area, stitching problems when registering scan patches, outliers and abnormal rough surfaces caused by calibration issues. We hypothesize that scans of poor-quality reach production because even trained personnel fail to correctly assess the scan's quality. Humans' incapability to properly evaluate scan quality has been observed in previous study [23].

To this day, this issue is a hindrance to business models centered on 3D scanning such as the novel 3Dscan-to-3Dprint business model; inadequate scans must be manually corrected by the operators of common software such as MeshLab™, MSoft™, MeshMixer™ and Geomagic™ [24], [25]. The use of these software is an offline process that is time consuming. In an orthotics and prosthetics central fab, it is not uncommon to process a 3D scan much later, when the patient has already left the O&P clinic. In case of a challenging 3D scan, the central fab technician must either perform a manual reconstruction of the knee (risking a product with a bad fit) or ask the clinician to reschedule an appointment to perform another 3D scan.

Moreover, handheld 3D scanners are poised to become common hardware with the potential of billions of devices integrating 3DS to a certain extent. Even if some attempts of integrating a 3D scanner inside a mobile phone have not been commercial success [26], they are now experiencing a forceful comeback as the general public can benefit from the added hardware for depth sensing for biometric authentication, augmented reality and depth effects in photographs; the iPhone X, X_R, X_S, 11 and 11 Pro now feature a frontal 3D scanner that can be used for 3D Scanning [27]. The sales of iPhone featuring a frontal 3D scanner now represents 37% of the U.S. mobile phone market [28], [29]. Other flagship such as the Samsung Note10+ now encompass similar technology [30], the innovation should continue both in terms of brand adoption as well as, in democratization.

This paper presents a study to quantify the reliability of the automatic reconstruction tool Shapeshift 3D Repair™ to create watertight, genus 0, precise and accurate 3D scans of the human body. Our methodology uses a precise baseline 3D scan as an input of a scanning process simulator that emulates the properties of a common 3D scanner, the Structure™ Sensor by Occipital™, and behavior of a typical untrained handheld 3D scanner operator. The output of the simulator is a raw scan (noisy with missing areas), such as illustrated on figure 3. Afterward, the raw scan is fed to Shapeshift 3D Repair™ which outputs a reconstructed scan. Using the girth difference between the baseline scan and reconstructed scan, we express the reliability of the process in terms of Standard Error of Measurement (SEM) and compatibility in terms of Signed Mean Difference (Bias) and Mean Absolute Error (MAE). We compare our results with common methods found in the literature and with other studies about the reliability of 3DS, PC and TA using rigorous statistical methodology based on [32].

2. Methods

2.1. Design of experiment

Full-body 3D scans were bought from a commercial source offering an end-user license compatible with the current usage. We have the template-fitted scans of 46 females and 55 males. The average triangle edge length of the original scan is 4.5 mm. We estimated the spatial trajectory of a handheld 3D scanner operated by an untrained operator and simulated the raw scan output of a Structure™ sensor. We then reconstructed the raw scan and compared it to the baseline scan. To measure the repeatability of Shapeshift 3D Repair™, three raw scans were generated per baseline scans; the experiment was designed to exceed the minimal sample size and repetition number for significantly testing H_0:p=0.8 versus H_1:p>0.8 [32]. The ICC was evaluated and compared to that of other reconstruction methods at the 5% significance level with 80% power. To better assess the reliability of our method, the one-sided 95% confidence interval lower bound ICC was determined.

2.1.1. Simulated trajectory hypothesis

The behavior of a typical untrained handheld 3D scanner operator was expressed in terms of the spatial trajectory he/she would do with the handheld device around the patient. It would best to extract real data from motion sensors of existing handheld 3D scanners to reconstruct the real spatial trajectory. However, applications such as 3DsizeME™ don't currently allow the extraction of the spatial trajectory.

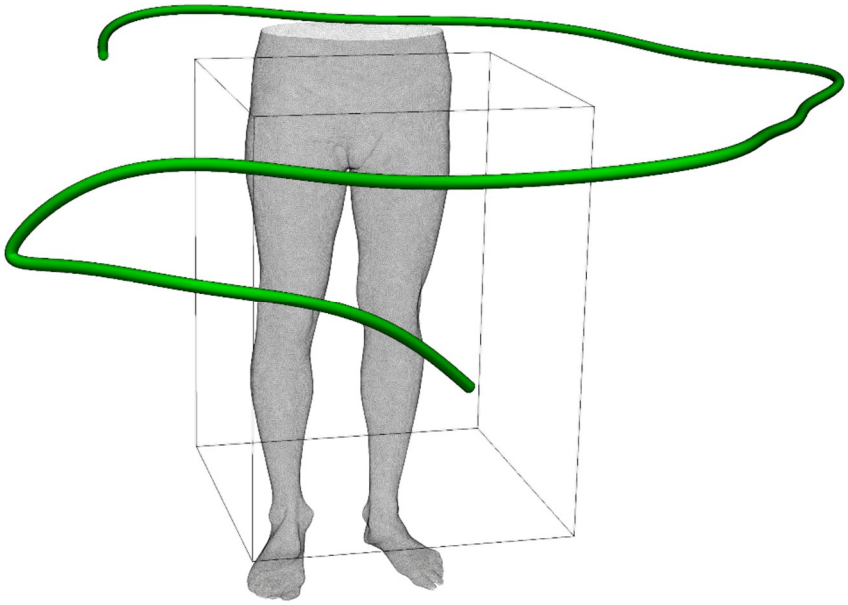

Figure 1. Simulated Trajectory for a left leg. Four different fields of views are shown as the handheld scanner travel along the trajectory.

As this information is not currently accessible, we took the approach of defining the trajectories. To emulate the scanning procedure of an untrained operator, assumptions are made: 1. Operators do not naturally walk in a perfectly circular trajectory; 2. To minimize efforts, scan operators hold the scanning device right in front of them, with the elbow bent at 90 degrees close to their abdomen and do not bend their knees; 3. 3D scan operators tend to oscillate between the social distance [32] and the recommended distance value recommended by apps such as 3DSizeMe which is 0.5 m; 4. Scan operators start in front of the targeted leg of the subject; 5. They then move medially toward the other leg to scan the medial part of the target leg before going in the opposite direction to scan its anterior, lateral and posterior part; 6. Normal scanning trajectory mostly stays in the XY plane, but some gait-related height variation happens during the whole process; 7. The scanner is always aimed at the knee.

These assumptions are converted into 7 basic hypotheses under which our simulated trajectory is defined: 1. Without noise, the trajectory is an ellipse; 2. The mean vertical position of the camera on its way back is about 20 cm above the knee; 3. The mean radius defining the trajectory is 0.6 m from the center 4. The trajectory starts perfectly in front of the targeted leg, facing the model; 5. The trajectory sweeps in the CW direction (left leg) or CCW direction (right leg) for 60 degrees, and then goes back for about 270 degrees; 6. Z-axis randomness is added on every point over which the cardinal spline is interpolated. 7. The simulated camera is always exactly looking at the center of the knee.

2.1.2. Definition of the simulated trajectory

The base trajectory is defined by a set of three independent unidimensional cardinal splines $S_x(i)$, $S_y(i)$, $S_z(i)$. Each cardinal spline is interpolated from a set of points $p_i, i \in [\![1, n]\!]$.

Given by both radius R_x(x-axis) and R_y(y-axis). Given the object we focus (right leg or left leg), centered at $O(x, y, z)$. Given a mean vertical position $h_z(i)$.

$$\begin{cases} S_x(i) = O_x + (R_x + \eta_x(i)) \sin(\mathrm{t(i)} + \theta_0) \\ S_y(i) = O_y + \left(R_y + \eta_y(i)\right) \sin(\mathrm{t(i)} + \theta_0) \\ S_z(i) = h_z(i) + \eta_z(i) \end{cases} \quad (1)$$

$$\text{Where } \theta_0 = \begin{cases} -160° & if\ right\ leg \\ -135° & if\ left\ leg \end{cases}$$

Every cardinal spline contains p points where $p = m + n$, where m is the number of points in the first direction and n, in the second direction.

Then, t takes values

$$t(i) = \begin{cases} t(i-1) - \frac{d}{2\pi} & i \in [\![1, m]\!] \\ t(i-1) + \frac{d}{2\pi} & i \in [\![m+1, n]\!] \\ 0 & i = 0 \end{cases} \quad (2)$$

$$\text{Where } d = \begin{cases} 1 & if\ right\ leg \\ -1 & if\ left\ leg \end{cases}$$

All the raw scans are generated using $m = 8$ and $n = 32$. The noise functions $\eta_x(i), \eta_y(i)$ are modeled on a normal distribution $N{\sim}(0, 25[cm])$, with a minimum distance cutoff value of 40 cm from the model. The noise function $\eta_z(i)$ is defined as $\eta_z(i) = \eta_x(i) \sin(\theta)$. Finally, once the control points are generated, we evaluate q points of the cardinal spline on a regular interval $t(i) = \frac{p-1}{q-1} i, i \in [\![1, q]\!]$, and insert them in the final trajectory $T(i) = \left(S_x(t(i)), S_y(t(i)), S_z(t(i))\right), i \in [\![1, q]\!]$.

All trajectories are generated using $q = 400$ points. Every point on the trajectory is equivalent to one "frame". Even if a traditional 3D scanner can process at least 54 frames per second, 400 points is enough to evaluate the areas that stayed hidden during the scanning process [33], and to define the noise level on the raw scans.

2.1.3. Raw scan extraction

A scanning process is subject to complex lighting patterns, wavelength absorption properties of materials, practically infinite definition of surfaces, porous, bumpy and hairy surfaces. Raw scans generated from our simulation will not consider these complex elements, but 5 other criteria are considered: 1. Angular threshold: Mesh points from surfaces too tangent to the scanner's orientation aren't detected by the scanner; 2. Field of view: Mesh points must be inside the FOV. Following hypothesis #7, the simulated 3D scanner is always focusing on the knee, the FOV is allowed vertical and transverse rotations but no longitudinal rotation. Using this information, the field of view of a Structure™ Sensor has a horizontal angle of 58 degrees and a vertical angle of 45 degrees; 3. Scanner emitter visibility: Mesh points must be visible to the emitter; 4. Scanner receiver visibility: Mesh points must be visible to the receiver. The scanner's emitter and receiver are distanced by $d = 6$ cm; 5. A box of dimensions 60 cm (depth) x 60 cm (width) x 80 cm (height) centered on the knee, acting as a filter.

For each position $T(i)$, we iterate through all points of the mesh to verify if it satisfies the 5 criteria. If satisfied, the point is considered as detected by the scanner. So, for every trajectory frame, we increment the count on the detected points. Finally, every point under 5 detections are removed from the mesh, generating the final raw scan.

2.1.4. Noise

On every trajectory frame, a randomly generated noise η_i is added on every raw scan point, following a normal distribution $N(\mu = 0, \sigma = P(d))$, where $P(d) = 0.000004060717 d^{1.97404}$ [34]. The total noise on every mesh point is given by:

$$\eta = \frac{\sqrt{\sum_{i=0}^{q} {\eta_i}^2}}{\sqrt{q}\sqrt{(q-1)}} \quad (3)$$

2.2. Data processing using 3D surface reconstruction methods

Our implementation consists of a cloud processing service via API. All compared reconstruction methods, including Shapeshift 3D Repair™, have for sole input a raw scan file. We compare Shapeshift 3D Repair™ with well-known reconstruction algorithms, the Power Crust algorithm and the Poisson reconstruction algorithm [35], [36]. Shapeshift 3D Repair™ add the requirement that scans height must be aligned with the third dimensional axis (Z-axis).

Due to the similarity in results between many software, we hypothesize that most open-source and close-source software use the Poisson reconstruction method as their surface reconstruction implementation. It seems to be the De Facto industry standard; however, the Poisson method produces mesh lacking certain desired properties. Advance modeling and CAD software require properly defined surface (manifold, genus 0, good triangle aspect ratio, single surface) to transform the surface in

NURBS representation. The Poisson method, by design, can't guarantee a watertight, genus 0 mesh with good triangle aspect ratio and a single surface. The Power Crust can guarantee a watertight mesh but cannot guarantee the genus 0 nor produce good mesh quality as indicated in Table 1. Moreover, the Power Crust can generate triangles with such bad aspect ratio that post-processing methods to improve the mesh quality might fail. Template base reconstruction method such as the 3D3D method by IBV guarantees good, high-quality mesh that are manifold, watertight and genus 0. However, they require a full-body scan to work and wouldn't work with the raw scan of the knee as define in this paper. Moreover, a full-body scan in a clinic environment is impractical, either with a full body 3D scanner or with a handheld device as one is costly and the other one is time inefficient especially when the region of interest is solely the knee.

Table 1. Qualitative comparison of 3D surface reconstruction methods.

Method	Manifold	Watertight	Genus 0	High quality mesh	Per-body part scanning	Single Surface
Shapeshift 3D Repair™	Y	Y	Y	Y	Y	Y
Power Crust	Y	Y	N	N	Y	N
Poisson	N	N	N	N	Y	N
IBV:3D3D	Y	Y	Y	Y	N	Y

2.4 Analytic procedures

For the reliability analysis, the leg girth was measured at 30 mm intervals from the knee axis. Positive position values are going upward, toward the abdomen and negative position value are going downward, toward the feet. As shown on Figure 2, circumference measurements are made on positions ranging from 180 mm to -180 mm.

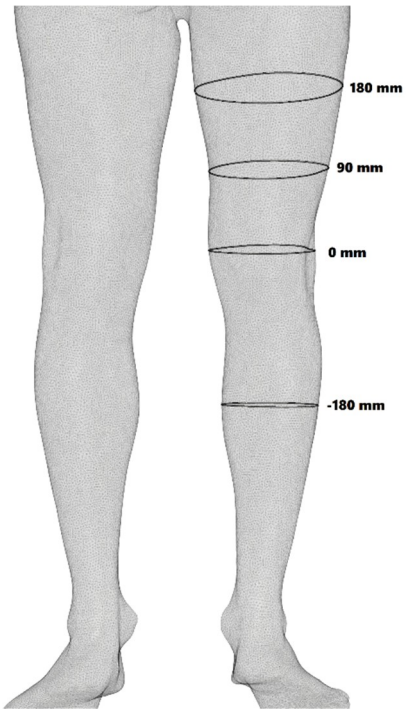

Figure 2. Circumference measurement position used for statistical analysis.

For the compatibility analysis, we estimated the Signed Mean Difference (Bias) and the Mean Absolute Error for each girth measurement between each method and the baseline scan. Moreover, we were able to calculate a maximum error limit on the circumference for each method using a 95% confidence interval.

Reconstructions with the Power Crust exhibited too much instability for precise statistical analysis to be conducted, the reconstructed mesh had holes and t-edges that made the automated measure extraction impossible.

3. Result and discussion

3.1 Reliability

In table 2A and 2B, we present the SEM and MAD for each 3D surface reconstruction method, from other Data-Driven 3D reconstruction methods (IBV:3D3D and IBV:2D3D) [38], and from the literature on TA methods [4],[39]-[48]. Figure 3 shows a baseline scan, one of the raw scans generated from it and the reconstruction from ShapeShift 3D Repair™. Figure 4 shows a baseline scan and the reconstructed scan with a color gradient representing the amplitude of the distance between each point on the reconstruction and the closest point on the baseline scan. Figure 5 shows a representative reconstruction of all listed algorithms alongside the baseline scan from which they reconstructed the raw scan.

Shapeshift Repair™ exhibits a 95% confidence interval lower bound ICC higher than 0.999 across all girth measurement, no matter their relative position to the knee. The reliability of the procedure can be observed on figure 7 which shows 3 raw scans generated from the same baseline scans alongside their reconstructions.

Table 2A. Standard Error of Measurement (SEM) in centimeters of different 3D surface reconstructions algorithms, Data-Driven 3D Reconstruction (D3DR) solutions (IBV:3D3D, IBV:2D3D) and TA.

Measurement	**Shapeshift 3D Repair™** MAD(SEM)	**Dirichlet-Poisson** MAD(SEM)	**Neumann-Poisson** MAD(SEM)	**Free-Poisson** MAD(SEM)
Max thigh girth (at 180mm)	(0.15)	(5.89)	(6.86)	(4.95)
Mid thigh girth (at 90mm)	(0.09)	(0.21)	(3.58)	(3.14)
Knee girth (at 0mm)	(0.09)	(0.09)	(0.09)	(0.09)
Leg girth (at -180mm)	(0.04)	(0.10)	(0.09)	(0.04)

Table 2B. Table 2A continued.

Measurement	**IBV:3D3D [38]** MAD(SEM)	**IBV:2D3D [38]** MAD(SEM)	**TA [4], [39]-[48]** MAD(SEM)
Max thigh girth (at 180mm)	0.10 (0.30)	0.30 (0.60)	0.3-0.9 (-)
Mid thigh girth (at 90mm)			
Knee girth (at 0mm)	0.10 (0.30)	0.20 (0.30)	0.26-0.33 (-)
Leg girth (at -180mm)			

Figure 3. A baseline scan (left), one raw scan generated from the baseline scan (middle) and its reconstruction using Shapeshift 3D Repair™(right).

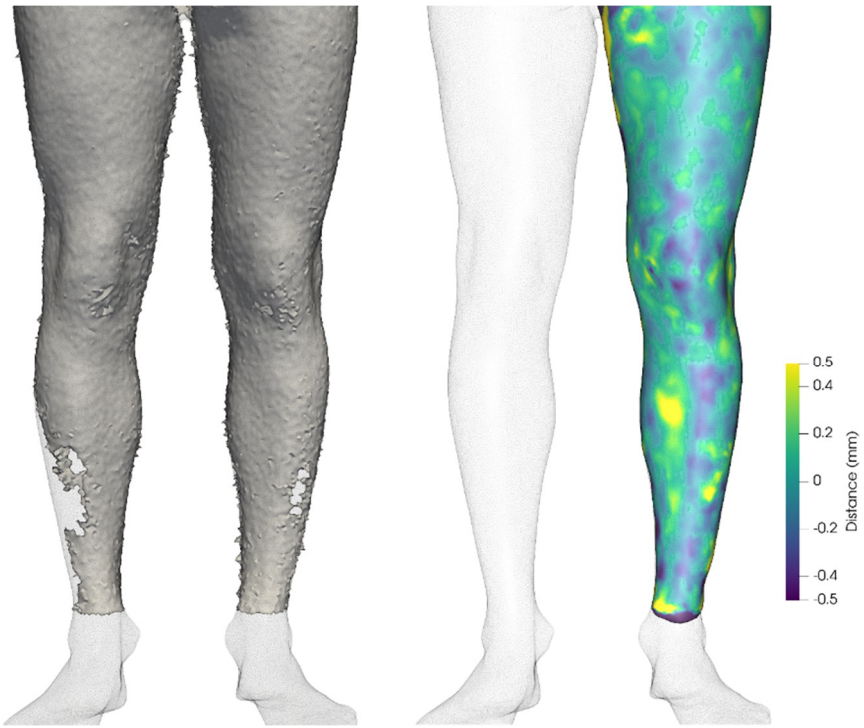

Figure 4. A baseline scan of the left leg (left) and a reconstructed scan (right) with a color gradient representing the distance between each point on the reconstructed scan and its closest point on the baseline scan.

Figure 5. Baseline scan of the left leg (left) and the related reconstruction from ShapeShift 3D Repair™, Dirichlet-Poisson, Free-Poisson, Neumann-Poisson and Power Crust methods in order, from left to right.

The table 2A and 2B demonstrate that Shapeshift 3D Repair™ has a better SEM than all listed methods, even in the case of an untrained operator, albeit simulated. Further improvement of Shapeshift 3D Repair™ should allow to obtain the same reliability across all girth measurements. The testing of both IBV methods and TA involves the scans of real humans which are prone to body sway and slight pose change [19], [49] while our method for testing 3D surface reconstruction methods are free of body sway and pose change.

The purpose of this article being the comparison of various algorithms to automatically reconstruct scans, no manual work was made to correct the results. This often results in methods other than Shapeshift 3D Repair™ filling the gap between the legs. Figure 6 displays an example of such gap filling by the Poisson Reconstruction algorithm. These artifacts explain the increasingly high SEM in other reconstruction methods as the measurement is made at higher relative position to the knee such as the Max thigh girth.

Figure 6. Gap filling between the legs caused by the Poisson algorithm.

Figure 7. Comparison of 3 raw scan generated from the same baseline scan and their reconstruction using Shapeshift 3D Repair™.

When compared to IBV:3D3D reconstruction (which necessitate, low-mobility, costly full body scanners), it is clear tha a handheld device that is poorly operated, but that scan exclusively the region of interest, which uses Shapeshift 3D Repair™ as reconstruction method can produce equally accurate or more accurate results than an expensive apparatus with a data-driven 3D reconstruction. When compared to another low-cost solution such as the IBV:2D3D method, which uses two photos with Age, Height and Weight, a poorly operated handheld 3D scan with Shapeshift 3D Repair™ have at least half of the error of the 2D3D method while not requiring any extra measurements [38].

3.2 Compatibility

In table 4, we compare the Bias and MAE between the baseline scan and the results of the different surface reconstruction methods, including results from IBV:2D3D and the Maximum Allowable Error extracted from the literature [2],[50]. Shapeshift 3D Repair™ has the best Bias and MAE across all girth measurements. All other studied automatic methods are over the Maximum Allowable Error. No data concerning the MAD and SEM of rectified plaster casts were found. Multiple casts of the same stump have been observed to have intra-prosthetist bias of up to 1.4 mm [51] which is equivalent to 0.9 cm girth bias. Following plaster casting, clinicians must perform cast rectification before manufacturing orthoses and prostheses. Inconsistency in rectifications of similar casts were observed intra and inter prosthetists: these variations can reach 2 mm and 1.5 mm in radius respectively. A 2 mm radius bias is equivalent to 1.3 cm girth bias. Both sources of distortion lead to inconsistency in plaster model shape and unreliable surface matching [52]. Such values of girth bias largely exceed the max allowable error [2],[50].

Table 4. Signed Mean Difference (Bias) and Mean Absolute Error (MAE) in centimeters between baseline scan and the different surface reconstruction methods, and between IBV:2D3D and 3D3D and Maximum Allowable Error from the literature.

Measurement	**Shapeshift 3D Repair™** Bias(MAE)	**Dirichlet-Poisson** Bias(MAE)	**Neumann-Poisson** Bias(MAE)	**Free-Poisson** Bias(MAE)	**IBV: 2D3D-3D3D [38]** Bias(MAE)	**Max. Allowable Error [2],[50]** Bias(MAE)
Max thigh girth (at 180mm)	0.13 (0.13)	32.4 (32.4)	32.2 (32.2)	32.0 (32.0)	-0.9 (1.3)	0.5 (0.6)
Mid thigh girth (at 90mm)	0.03 (0.04)	7.4 (7.4)	7.2 (7.2)	7.1 (7.1)		
Knee girth (at 0mm)	0.1 (0.1)	2.2 (2.2)	2.2 (2.2)	2.1 (2.1)	-0.8 (1.2)	0.5 (0.5)
Knee girth (at --180mm)	0.03 (0.03)	0.14 (0.15)	0.13 (0.14)	0.04 (0.4)		

As shown in table 5, our fully digital testing methodology allows us to define an upper limit on the absolute maximum error limit on the circumference using a 95% confidence interval. We also compared with the Bias and SEM of the absolute maximum error limit between the baseline IBV:3D3D and the IBV:2D3D method.

*Table 5. Absolute maximum error limits on the circumference. |Bias|+1.96*SEM in centimeters.*

Measurement	**Shapeshift 3D Repair™**	**Dirichlet-Poisson**	**Neumann-Poisson**	**Free-Poisson**	**IBV:2D3D-3D3D**
Max thigh girth (at 180mm)	0.42	43.9	45.6	41.7	2.1
Mid thigh girth (at 90mm)	0.22	7.87	14.2	13.3	
Knee girth (at 0mm)	0.29	1.92	1.89	1.41	1.4
Knee girth (at --180mm)	0.11	0.35	0.31	0.12	

Shapeshift 3D Repair™ reconstruction offer lower absolute maximum error, BIAS and SEM for all girth measurements.

4. Conclusion and further work

Through this study, Shapeshift 3D Repair™ has demonstrated the ability to create reliable 3D scans using handheld 3D scanner considering a user that hasn't follow a thorough training program, albeit simulated in our study. An untrained user can create knee scans that respect than the maximum allowable error [2], [50] with leg, knee and max thigh girth error respectively under 0.1 cm, 0.3 cm and 0.4 cm with 95% confidence level while producing properly defined surface that are manifold, genus 0, have good triangle aspect ratio, and have a single surface. The surface can be easily imported into any CAD package to create 3Dscan-to-3Dprint devices.

A fully automated and unsupervised cloud processing service for the reconstruction of the knee has been implemented and is ready to be tested by users and vendors of 3D scanners. With the recent boom of devices featuring an embedded 3D scanner, we believe that in due time, our technology can be accessible to millions of users without the needs of industry-specific hardware or skills.

References

[1] C. C. Gordon and B. Bradtmiller, “Interobserver error in a large scale anthropometric survey,” *Am. J. Hum. Biol.*, vol. 4, no. 2, pp. 253–263, 1992. https://doi.org/10.1002/ajhb.1310040210

[2] C. C Gordon *et al.*, “Anthropometric Survey of U.S. Army Personnel: Summary Statistics, Interim Report for 1988,” Jan. 1989.

[3] M. Kouchi, M. Mochimaru, K. Tsuzuki, and T. Yokoi, “Random errors in anthropometry,” *J Hum Ergol (Tokyo)*, vol. 25, no. 2, pp. 155–166, Dec. 1996.

[4] M. Kouchi and M. Mochimaru, “Evaluation of Accuracy in Traditional and 3D Anthropometry,” SAE International, Warrendale, PA, SAE Technical Paper 2008-01–1882, Jun. 2008. https://doi.org/10.4271/2008-01-1882

[5] J.H. Tyo and R.D. Koch, “Procedures For Obtaining Casts For Ankle-Foot Orthoses,” *O&P Virtual Library*, vol. 32, no. 2, pp. 12–20, 1978.

[6] D. Pod, “Cost benefit comparison of plaster casts and optical scans of the foot for the manufacture of foot orthoses,” *AJPM*, vol. 41, no. 2, pp. 29–31, 2007.

[7] M. Carroll, M.-E. Annabell, and K. Rome, “Reliability of capturing foot parameters using digital scanning and the neutral suspension casting technique,” *Journal of Foot and Ankle Research*, vol. 4, no. 1, p. 9, Mar. 2011. https://doi.org/10.1186/1757-1146-4-9

[8] A. Kuehnapfel, P. Ahnert, M. Loeffler, A. Broda, and M. Scholz, “Reliability of 3D laser-based anthropometry and comparison with classical anthropometry,” *Sci Rep*, vol. 6, 26 2016. https://doi.org/10.1038/srep26672

[9] “The World’s First 3D Printed Custom Knee Brace”, *OssKin*, http://www.osskin.com., accessed 2019.

[10] *Unlimited Tomorrow*, https://www.unlimitedtomorrow.com., accessed 2019.

[11] A. Ballester *et al.*, “3D-Based Resources Fostering the Analysis, Use, and Exploitation of Available Body Anthropometric Data,” 2014. https://doi.org/10.15221/14.237

[12] A. Ballester *et al.*, “3D Body Databases of the Spanish Population and its Application to the Apparel Industry,” 2015. https://doi.org/10.15221/15.232

[13] D. Lacko *et al.*, “Ergonomic design of an EEG headset using 3D anthropometry,” *Appl Ergon*, vol. 58, pp. 128–136, Jan. 2017. https://doi.org/10.1016/j.apergo.2016.06.002

[14] S. Verwulgen *et al.*, “A new data structure and workflow for using 3D anthropometry in the design of wearable products,” *International Journal of Industrial Ergonomics*, vol. 64, pp. 108–117, Mar. 2018. https://doi.org/10.1016/j.ergon.2018.01.002

[15] W. Lee *et al.*, “Application of massive 3D head and facial scan datasets in ergonomic head-product design,” *International Journal of the Digital Human*, vol. 1, p. 344, Dec. 2016. https://doi.org/10.1504/ijdh.2016.10005368

[16] A. Haleem and Mohd. Javaid, “3D scanning applications in medical field: A literature-based review,” *Clinical Epidemiology and Global Health*, vol. 7, no. 2, pp. 199–210, Jun. 2019. https://doi.org/10.1016/j.cegh.2018.05.006

[17] M. Hassmann, S. Stoeger, J. Dastl, and W. Krach, “Scanning Procedure of Female Torso Using Low-Cost Hand-Held Sense 3D Scanner,” presented at the Proc. of 3DBODY.TECH 2018 - 9th Int. Conference and Exhibition on 3D Body Scanning and Processing Technologies, Lugano, Switzerland, 16-17 Oct. 2018, 2018. http://dx.doi.org/10.15221/18.074

[18] L. S. Chapman *et al.*, “Foot orthoses for people with rheumatoid arthritis: a survey of prescription habits among podiatrists,” *Journal of Foot and Ankle Research*, vol. 12, no. 1, p. 7, Jan. 2019. https://doi.org/10.1186/s13047-019-0314-5

[19] M. Kouchi and M. Mochimaru, “Errors in landmarking and the evaluation of the accuracy of traditional and 3D anthropometry,” *Appl Ergon*, vol. 42, no. 3, pp. 518–527, Mar. 2011. https://doi.org/10.1016/j.apergo.2010.09.011

[20] D. Anguelov, P. Srinivasan, D. Koller, S. Thrun, J. Rodgers, and J. Davis, “SCAPE: Shape Completion and Animation of People,” in *ACM SIGGRAPH 2005 Papers*, New York, NY, USA, 2005, pp. 408–416. https://doi.org/10.1145/1186822.1073207

[21] D. A. Hirshberg, M. Loper, E. Rachlin, and M. J. Black, “Coregistration: Simultaneous Alignment and Modeling of Articulated 3D Shape,” in *Computer Vision – ECCV 2012*, 2012, pp. 242–255. https://doi.org/10.1007/978-3-642-33783-3_18

[22] M. Loper, N. Mahmood, J. Romero, G. Pons-Moll, and M. J. Black, “SMPL: a skinned multi-person linear model,” *ACM Trans. Graph.*, vol. 34, pp. 248–248, 2015. http://doi.org/10.1145/2816795.2818013

[23] X. Yin, B. D. Corner, and A. Razdan, “EARS: Toward Fast Analysis of 3D Human Scans,” 2010.

[24] D. F. Redaelli, S. Gonizzi Barsanti, P. Fraschini, E. Biffi, and G. Colombo, “LOW-COST 3D DEVICES AND LASER SCANNERS COMPARISON FOR THE APPLICATION IN ORTHOPEDIC CENTRES,” *ISPRS - International Archives of the Photogrammetry, Remote Sensing and Spatial Information Sciences*, vol. XLII–2, pp. 953–960, May 2018. https://dx.doi.org/10.5194/isprs-archives-XLII-2-953-2018

[25] E. S. Schrank and S. J. Stanhope, “Dimensional accuracy of ankle-foot orthoses constructed by rapid customization and manufacturing framework.,” *Journal of rehabilitation research and development*, vol. 48, no. 1, pp. 31–42, 2011. https://doi.org/10.1682/jrrd.2009.12.0195

[26] “ProBeat: Google killed the first Daydream and Tango phone after less than a month,” *VentureBeat*, 01-Sep-2017.

[27] *Standard Cyborg*, https://www.standardcyborg.com/profile., accessed 2019.

[28] “Mobile Vendor Market Share United States Of America” *StatCounter Global Stats*, https://gs.statcounter.com/vendor-market-share/mobile/united-states-of-america., accessed 2019.

[29] “Apple’s iPhone XR was the best Selling Smartphone in the U.S. in Q2 with a Whopping 48% Market Share,” *Patently Apple*, https://www.patentlyapple.com/patently-apple/2019/07/apples-iphone-xr-was-the-best-selling-smartphone-in-the-us-in-q2-with-a-whopping-48-market-share.html., accessed 2019.

[30] “Samsung Galaxy Note 10,” *Wikipedia*. 30-Aug-2019.

[31] F. Commandeur, J. Velut, and O. Acosta, “A VTK Algorithm for the Computation of the Hausdorff Distance,” *The VTK Journal*, p. 839, Sep. 2011.

[32] M. Eliasziw, S. Young, M. G. Woodbury, and K. Fryday-Field, “Statistical Methodology for the Concurrent Assessment of Interrater and Intrarater Reliability: Using Goniometric Measurements as an Example,” Physical therapy, vol. 74, pp. 777–88, Sep. 1994. https://doi.org/10.1093/ptj/74.8.777

[33] Edward T. Hall, The Hidden Dimension. Anchor, 1990.

[34] “Specs & Data”, Structure by Occipital, https://structure.io/structure-core/specs., accessed 2019.

[35] “How precise is the Structure Sensor?”, Structure by Occipital, https://support.structure.io/article/158-how-precise-is-the-structure-sensor., accessed 2019.

[36] N. Amenta, S. Choi, and R. K. Kolluri, “The Power Crust,” in Proceedings of the Sixth ACM Symposium on Solid Modeling and Applications, New York, NY, USA, 2001, pp. 249–266. http://doi.org/10.1145/376957.376986

[37] M. Kazhdan, M. Bolitho, and H. Hoppe, “Poisson Surface Reconstruction,” in Proceedings of the Fourth Eurographics Symposium on Geometry Processing, Aire-la-Ville, Switzerland, Switzerland, 2006, pp. 61–70.

[38] A. Ballester et al., “3D Human Models from 1D, 2D and 3D Inputs: Reliability and Compatibility of Body Measurements,” 2018, pp. 132–141. http://dx.doi.org/10.15221/18.132

[39] N. Koepke et al., “Comparison of 3D laser-based photonic scans and manual anthropometric measurements of body size and shape in a validation study of 123 young Swiss men,” PeerJ, vol. 5, Feb. 2017. https://dx.doi.org/10.7717%2Fpeerj.2980

[40] B. K. Ng, B. J. Hinton, B. Fan, A. M. Kanaya, and J. A. Shepherd, “Clinical anthropometrics and body composition from 3D whole-body surface scans,” Eur J Clin Nutr, vol. 70, no. 11, pp. 1265–1270, 2016. https://doi.org/10.1038/ejcn.2016.109

[41] J. Wang, D. Gallagher, J. C. Thornton, W. Yu, M. Horlick, and F. X. Pi-Sunyer, “Validation of a 3-dimensional photonic scanner for the measurement of body volumes, dimensions, and percentage body fat,” Am J Clin Nutr, vol. 83, no. 4, pp. 809–816, Apr. 2006. https://dx.doi.org/10.1093%2Fajcn%2F83.4.809

[42] T. E. VONK and H. Daanen, “Validity and Repeatability of the Sizestream 3D Scanner and Poikos Modeling System,” 2015, pp. 293–299. http://dx.doi.org/10.15221/15.293

[43] J. C. K. Wells et al., “Acceptability, Precision and Accuracy of 3D Photonic Scanning for Measurement of Body Shape in a Multi-Ethnic Sample of Children Aged 5-11 Years: The SLIC Study,” PLoS ONE, vol. 10, no. 4, 2015. https://doi.org/10.1371/journal.pone.0124193

[44] M. R. Pepper et al., “Validation of a 3-dimensional laser body scanner for assessment of waist and hip circumference,” J Am Coll Nutr, vol. 29, no. 3, pp. 179–188, Jun. 2010.

[45] Ł. Markiewicz, M. Witkowski, R. Sitnik, and E. Mielicka, “3D anthropometric algorithms for the estimation of measurements required for specialized garment design,” Expert Systems with Applications, vol. 85, pp. 366–385, Nov. 2017. https://doi.org/10.1016/j.eswa.2017.04.052

[46] J. Lu and M. J. Wang, “The Evaluation of Scan-Derived Anthropometric Measurements,” IEEE Transactions on Instrumentation and Measurement, vol. 59, no. 8, pp. 2048–2054, Aug. 2010. https://doi.org/10.1109/TIM.2009.2031847

[47] K. Yamauchi, B. Bhanu, and H. Saito, “3D Human Body Modeling Using Range Data,” in 2010 20th International Conference on Pattern Recognition, 2010, pp. 3476–3479. https://doi.org/10.1109/ICPR.2010.849

[48] K. M. Robinette and H. A. M. Daanen, “Precision of the CAESAR scan-extracted measurements,” Appl Ergon, vol. 37, no. 3, pp. 259–265, May 2006. https://doi.org/10.1016/j.apergo.2005.07.009

[49] H. A. M. Daanen and A. Psikuta, “10 - 3D body scanning,” in Automation in Garment Manufacturing, R. Nayak and R. Padhye, Eds. Woodhead Publishing, 2018, pp. 237–252. https://doi.org/10.1016/B978-0-08-101211-6.00010-0

[50] ISO 20685:2010 - 3-D scanning methodologies for internationally compatible anthropometric databases. 2010

[51] A. W. P. Buis, A. Blair, P. Convery, S. Sockalingam, and B. McHugh, “Pilot study: data-capturing consistency of two trans-tibial casting concepts, using a manikin stump model: a comparison between the hands-on PTB and hands-off ICECAST compact concepts,” Prosthet Orthot Int, vol. 27, no. 2, pp. 100–106, Aug. 2003. https://doi.org/10.1080/03093640308726665

[52] P. Convery, A. W. P. Buis, R. Wilkie, S. Sockalingam, A. Blair, and B. McHugh, “Measurement of the consistency of patellar-tendon-bearing cast rectification,” Prosthet Orthot Int, vol. 27, no. 3, pp. 207–213, Dec. 2003. https://doi.org/10.1080/03093640308726683